Pertanika J. Sci. & Technol. 25 (3): 1019 - 1028 (2017)

SCIENCE & TECHNOLOGY

Journal homepage: http://www.pertanika.upm.edu.my/

A Computational Fluid Dynamics Study of Combustion and Emission Performance in an Annular Combustor of a Jet Engine

M. Zuber[1]*, M. S. B. Hisham[2], N. A. M. Nasir[2], A. A. Basri[2] and S. M. A. Khader[3]

[1]Department of Aeronautical and Automobile Engineering, Manipal Institute of Technology, Manipal University, Manipal 576104, India

[2]Department of Aerospace Engineering, Faculty of Engineering, Universiti Putra Malaysia, 43400 UPM, Serdang, Selangor, Malaysia

[3]Department of Biochemistry, School of Biomedical Sciences, The University of Hong Kong, Pokfulam, Hong Kong

ABSTRACT

This paper is a Computational Fluid Dynamics (CFD) study of the performance of a jet engine annular combustor that was subjected to various loading conditions. The aim is to comprehend the effect of various genuine working conditions on ignition and emission performance. The numerical models utilized for fuel ignition is the feasible k-ω model for turbulent stream, species transport (aviation fuel and air) with eddy-dissipation reaction modelling and pollution model for nitrogen oxides (NO_X) emission. The results obtained confirm the findings described in the literature.

Keywords: Annular combustor, CFD, combustor loading, jet engine, gas emission

INTRODUCTION

Gas turbines operating at simple cycle have low efficiencies due to the loss of energy to the atmosphere (Alves & Nebra, 2003). The combustor is the hottest part of the gas turbine thus frequent use affects its lifespan (Li, Peng, & Liu, 2006). Many studies have been carried out to improve the performance of a gas turbine (Alves & Nebra, 2003; Carapellucci & Milazzo, 2005; Luo, Zhang, Lior, & Lin, 2011; Han, Jin, Zhang, & Zhang, 2007). Li et al., 2006 utilized the CFD model to analyse the ignition and cooling in an air motor combustor. Wang, Luo, Lu and Fan (2011) considered the structure of a hydrogen/air premixed fire in a small-scale combustor using the direct numerical simulation method. Gobbato, Masi, Toffolo and Lazzaretto (2011) performed a

Article history:
Received: 11 January 2017
Accepted: 21 April 2017

E-mail addresses:
mdzubairmanipal@gmail.com, mohammad.zuber@manipal.edu (M. Zuber),
syafiqbad94@gmail.com (M. S. B. Hisham),
athrhnsr@gmail.com (N. A. M. Nasir),
adi.azriff@gmail.com (A. A. Basri),
smak.quadri@gmail.com (S. M. A. Khader)
*Corresponding Author

ISSN: 0128-7680

CFD reproduction on a hydrogen fuelled single can gas turbine combustor. Ghenai (2010) completed a numerical examination on the combustion of syngas fuel blend in gas turbine can combustor. The impact of syngas fuel composition and lower heating value on the fire shape, gas temperature, and nitrogen oxides per unit of energy generation were also studied. Zhang, Fu, Lin and Li (2012) examined the NO_X emanation in a model commercial aircraft motor combustor using CFD. The present study investigates the can annular combustor in order to understand its working at various loading conditions and examine the NOx and CO_2 emissions during operation.

METHOD

Governing Equations

The mathematical equations to show combustion depend on the equations of conservation of mass, momentum, and energy together with other supplementary equations for the turbulence and combustion. The SST k-ω turbulence model is utilized as a part of this study. The equations for the turbulent kinetic energy k and the specific dissipation rate of the turbulent kinetic energy ω are solved. The reaction model is activated with species transport. The radiation effects are ignored. The equations are as follows (Mujeebu, Abdullah, & Zubair, 2013; Ismail et al., 2013).

Mass Conservation Equation:

$$\frac{\partial \rho}{\partial t} + \nabla \cdot \left(\rho \vec{V} \right) = S_m \tag{1}$$

Where the S_m is the mass added to the continuous phase from the dispersed second phase.

Continuity Equation:

$$\frac{\partial \rho}{\partial t} + \frac{\partial}{\partial x}\left(\rho v_x \right) + \frac{\partial}{\partial r}\left(\rho v_r \right) + \frac{\rho v_r}{r} = S_m \tag{2}$$

Where x is the axial coordinate, r is the radial coordinate, v_x is the axial velocity, and v_r is the radial velocity.

Momentum Conservation Equations:

$$\frac{\partial}{\partial t}(\rho \vec{v}) + \nabla \cdot (\rho \vec{v}\vec{v}) = -\nabla \rho + \nabla \cdot (\bar{\bar{\tau}}) + \rho \vec{g} + \vec{F} \tag{3}$$

Where $\bar{\bar{\tau}}$ is the stress tensor, $\rho \vec{g}$ and $\vec{F}$ are the gravitational body force and external body forces, respectively.

Species Transport Model:

$$\frac{\partial}{\partial t}\left(\rho Y_i \right) + \nabla \cdot \left(\rho \vec{v} \vec{Y_i} \right) = -\nabla \cdot \vec{J_i} + R_i + S_i \tag{4}$$

Where R_i the net is rate of production by chemical reaction and S_i is the rate of creation by addition from the dispersed phase plus any user defined sources.

Transport Equations for the SST k-ω model:

$$\frac{\partial}{\partial t}(\rho k)+\frac{\partial}{\partial x_i}(\rho k u_i)=\frac{\partial}{\partial x_j}\left(\Gamma_k \frac{\partial k}{\partial x_j}\right)+G_k-Y_k+S_k \tag{5}$$

$$\frac{\partial}{\partial t}(\rho \omega)+\frac{\partial}{\partial x_j}(\rho \omega u_j)=\frac{\partial}{\partial x_j}\left(\Gamma_\omega \frac{\partial \omega}{\partial x_j}\right)+G_\omega-Y_\omega+D_\omega+S_\omega \tag{6}$$

Where the term G_k represents the production of turbulence kinetic energy, and is defined in the same manner as in the standard k-ω model. G_ω represents the generation of ω. Γ_k and Γ_ω represent the effective diffusivity of k and ω, respectively. Y_k and Y_ω represent the dissipation of k and ω due to turbulence. D_ω represents the cross-diffusion term. S_k and S_ω are user-defined source terms.

$$\sigma_{k1}=0.85, \sigma_{k2}=1, \sigma_{\omega 1}=0.5, \sigma_{\omega 2}=0.856$$

Geometry, Boundary Conditions, Mesh and Numerical Method

The basic geometry of the gas turbine annular combustor is shown in the Figure 1(a). The size of the combustor is 0.341 m in the Y direction and 0.65 m in the X direction. The dimensions of the combustor were obtained from the works of (Chaudhari, Kulshreshtha, & Channiwala, 2012). A quality mesh was generated for the annular combustor and the mesh dependency study resulted in the mesh count of 41605 elements.

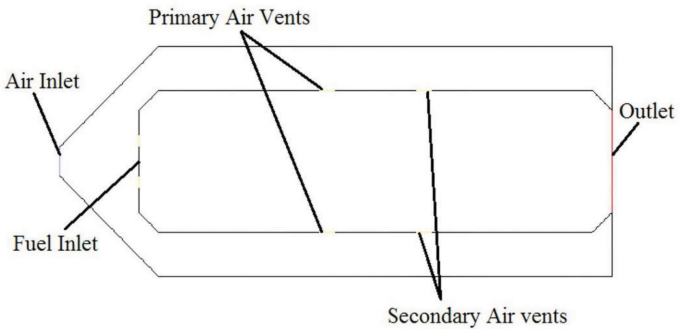

Figure 1. 2D model of the gas turbine annular combustor

The finite volume method and the second order upwind method were used to solve the governing equations. The convergence criteria were set to 10^{-4} for the mass, momentum, turbulent kinetic energy, dissipation rate of turbulent kinetic energy and the mixture fraction.

For the energy and the pollution equations, the convergence criteria were set to 10^{-6}. The boundary conditions of the air and fuel are similar to the one presented by Gang and Hongtao (2013) and are shown in Table 1.

Table 1
Combustor conditions

Condition	Mass flow rate of air (kg/s)	Temperature of air (K)	Mass flow rate of fuel (kg/s)	Temperature of fuel (K)	Combustor load %
1	2.7568	645.4	0.04184	305	30
2	3.3458	693.2	0.05939	305	50
3	3.8096	726.8	0.07552	305	70
4	4.016	742	0.08382	305	80
5	4.3865	769.9	0.09987	305	100

The experiment data of Dang (2009), was utilized to validate the numerical findings. In the experimental and numerical cases, the fuel of aviation kerosene was considered. The boundary condition of the experimental and numerical cases are follows: the temperature is 500K, mass flow rate of air 0.24 kg/s,, mass flow rate of fuel 0.0624 kg/s, and the fuel temperature 305K.

RESULTS AND DISCUSSIONS

Validation with Literature

The CO_2 mass fraction and the temperature radial profiles at the combustor outlet was compared with the results of Dang (2009), in Figure 2, respectively. The value of CO_2 mass fraction and temperature in the present results and the experimental results of Dang (2009), were similar.

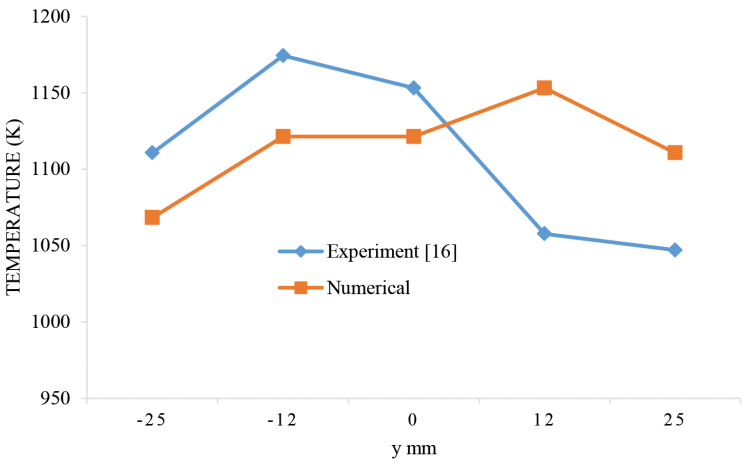

(a) Temperature

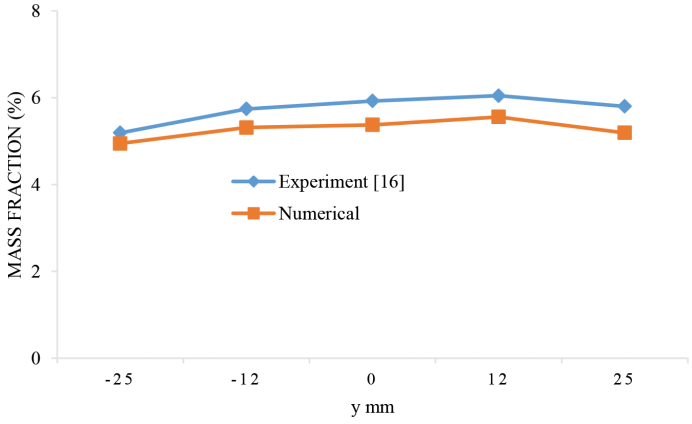

(b) CO_2 mass fraction

Figure 2. CO_2 mass fraction radial profile and temperature at combustor outlet

Flow field

The velocity field in the combustor under condition 5 is shown in Figure 3. The streamlines indicate the path followed by the air and fuel under conditions 1 to 5 are identical with only a marginal difference. In this study, only the streamlines for condition 5 are depicted. Air flow from the inlet to the combustor outlet can be divided into two zones, namely primary zone, and secondary zone.

In the primary zone, the air leaves the inlet to the combustor liner at high velocity. The air mixes with fuel injected from the nozzle, flows forward and entraps the air in the centre of the combustor liner while the downstream air refills the region. As a result, a central recirculation zone with a counter rotating vortex pair forms in the head of the combustor liner, and ensures the burning and stable combustion in the combustor liner. Due to symmetry of the shell, the air flow rates into the combustor liner from the upper and lower surfaces are also symmetric.

In the downstream area of the primary zone, strong fresh air is injected into the combustor liner from the primary holes; as a result, the primary zone is cut off by the fresh air. Although a small amount of gas is inhaled into the primary zone, most of it flows downstream to mix with the cold air from the secondary zone. This results in more uniform flow in the combustor.

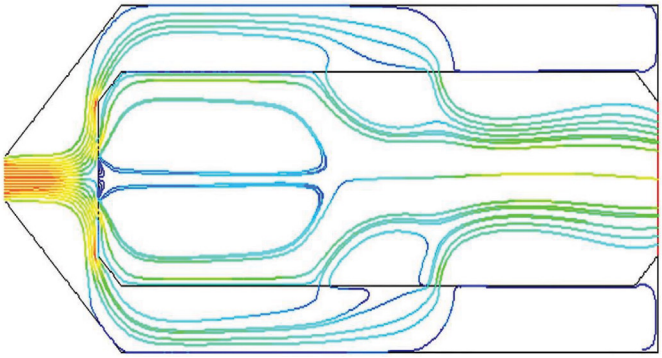

Figure 3. Streamline velocity of condition 5

The air flow distribution is a fundamental issue in combustor configuration and advancement. It influences the combustor ignition, combustion productivity, fire stability, absolute pressure loss, wall cooling, as well as the outlet temperature distribution. Figure 4 demonstrates the extent of primary zone air conveyance. It can be seen from the figure, the proportion of air circulation under various conditions are similar: air inlet=15%, primary air = 29.5%. It can be presumed that the air circulation is for the most part dictated by the combustor structure, not the working conditions.

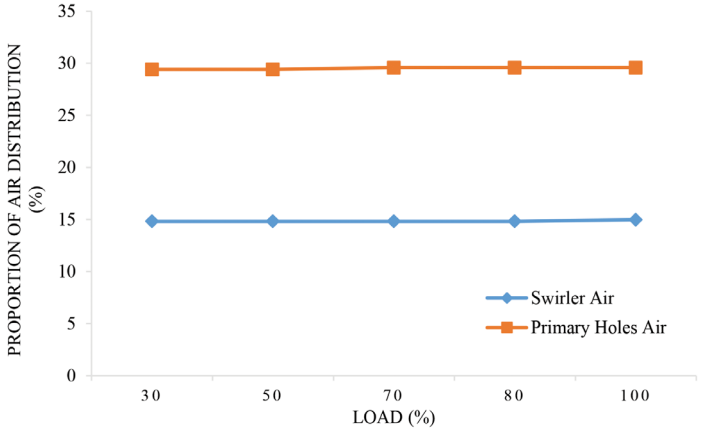

Figure 4. Flow distribution of air in different conditions

Temperature Field

The contours of the anticipated gas temperature for the combustion of fuel aviation kerosene in combustor are explained in Figure 5. The highest gas temperature is mostly concentrated at the tail end of the exit of the combustor. The temperature at the primary combustion zone is in the range of 1900 to 2100K for all the loading conditions. At higher loads, the combustor temperature is quite less and the maximum temperature region is pushed towards the exit tail. It is on the grounds that more fuel is burned in the combustor under the high load. The temperature of the gas close to the lower surface of the combustor liner is lower than that close to the upper surface in the centre zone and mixing zone

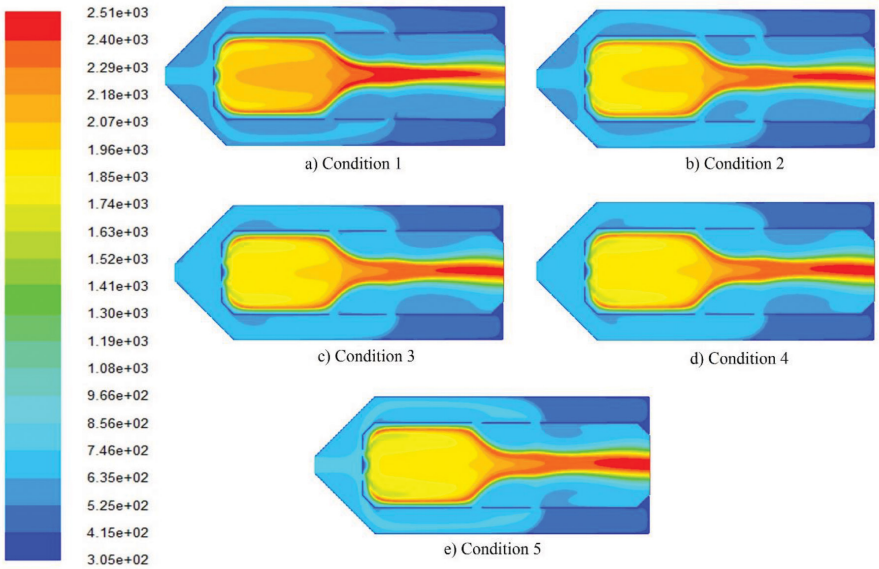

Figure 5. Contour of Temperature

As seen from Figure 5, there are two high temperature zones in the combustor. One is at the centre and where the temperature increases with the load along the central axis of combustor liner. The other located behind the primary zones, which only exists when the air-fuel mixture is above 30% load, and gets higher as the load increases. No significant change in the temperature along the central axis of the combustor as observed as per Figure 6. This shows that, higher loads have less effect on the performance of the combustor. However, there is a significant increase downstream suggesting higher load increases the exit temperature of the combustor gases.

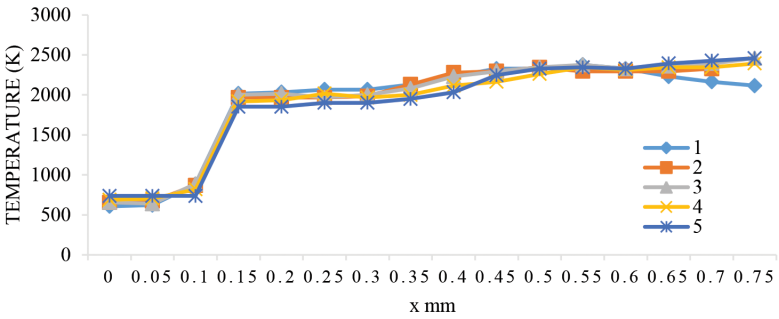

Figure 6. Central axis of temperature distribution

Emission

NO_x Emission. Figure 7 shows the production of NO_X discharge at combustor outlet for different operating conditions indicated in Table 1. The least NO_X outflow is 444.44 ppm at condition 1 and the most elevated is 623.98 ppm at condition 5. The higher temperature in the primary zone can increase the production of NOx and is evident with increased temperature associated with condition 5, more NOx was produced.

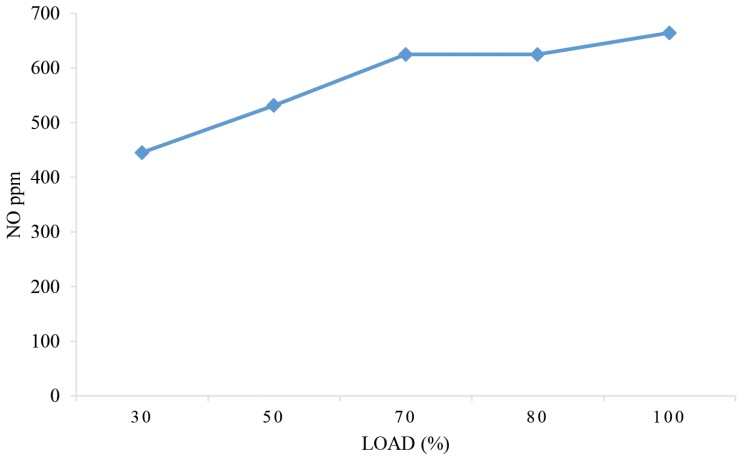

Figure 7. Emission of NO_X at outlet in different condition

CO_2 Emission. Figure 8 shows the mass fraction of CO_2 in the core of combustor in 100% load (Condition 5). It can be inferred that CO_2 distribution follows the similar pattern as that of temperature and maximum CO2 can be observed at the downstream region. The increase in load also increases the CO2 production as observed from the Figure 9. The mass fraction of CO_2 having maximum of 0.0746 kg was obtained at condition 5 and lowest of 0.0537 kg at condition 1.

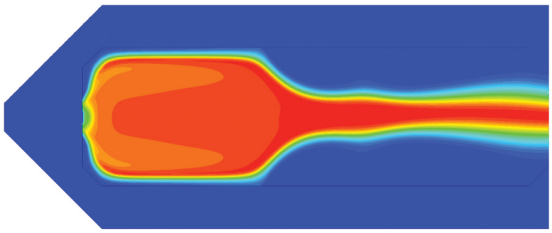

Figure 8. Contour of mass fraction CO_2 (Condition 5)

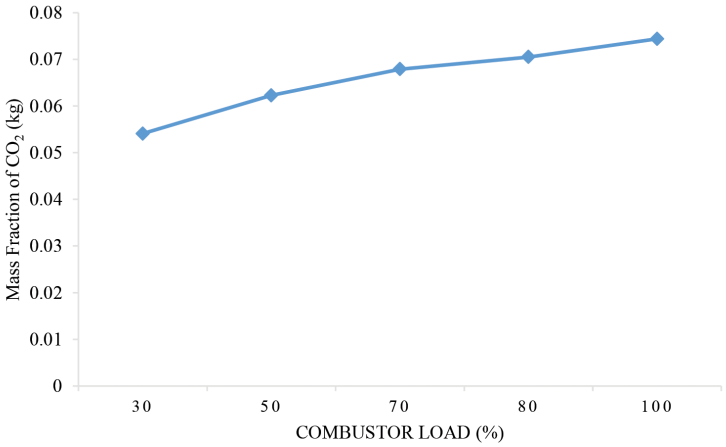

Figure 9. Mass fraction of CO_2 at the outlet in various condition

CONCLUSIONS

The two-dimensional CFD study of combustion in jet engine annular combustor performed in this study are as follows:

1) The combustor burns fuel viably under various conditions. A core of combustor chamber with different angle of primary and secondary inlet could improve the flame stability under different conditions.
2) Because of the symmetrical flow field, the temperature conveyance in combustor is symmetrical too. The gas temperatures close to the upper and lower surfaces of combustor liner are identical, and the greatest temperature contrast is around 100K in the centre zone for each condition, which is helpful to secure the liner. Hence, a symmetrical stream field in the combustor may expand the life of the combustor liner.
3) The estimations of the NO_X outflow are 623.98 ppm and 444.4 ppm under 100% load and 30% load respectively. It is also observed that there is an increase in CO_2 emission with increase in the load.

ACKNOWLEDGEMENTS

The authors would like to thank Universiti Putra Malaysia (UPM) for providing funds through the UPM GP –IPM/2014/9444000 grant.

REFERENCES

Alves, L. G., & Nebra, S. A. (2003). Thermoeconomic evaluation of a basic optimized chemically recuperated gas turbine cycle. *International Journal of Thermo-dynamics, 6*(1), 13–22.

Carapellucci, R., & Milazzo, A. (2005). Thermodynamic optimization of a reheat chemically recuperated gas turbine. *Energy Conversion and Management, 46*(18-19), 2936–2953.

Chaudhari, K. V., Kulshreshtha, D. B., & Channiwala, S. A. (2012). Design and CFD simulation of annular combustion chamber with kerosene as fuel for 20 kW gas turbine engine. *International Journal of Engineering Research and Applications (IJERA), 2*(6), 1641-1645.

Chen, J. C., & Chen, W. (2012). How flow becomes turbulent. *IAENG International Journal of Applied Mathematics, 42*(2), 99–110.

Danao, L. A., Edwards, J., Eboibi, O., & Howell, R. (2013). A numerical investigation into the effects of fluctuating wind on the performance of a small scale vertical axis wind turbine. *Engineering Letters, 21*(3), 149–157.

Dang, X. X. (2009). *Experimental investigation and numerical simulation of a gas turbine annular combustor with dual-stage swirler*. (Doctoral thesis). Nanjing University of Aeronautics and Astronautics.

Gang, P., & Hongtao, Z. (2013). Combustion and emission performance in a can annular combustor. *Engineering Letters, 22*(1), EL_22_1_03.

Ghenai, C. (2010). Combustion of syngas fuel in gas turbine can combustor. *Advances in Mechanical Engineering, 2010*, 1–13.

Gobbato, P., Masi, M., Toffolo, A., & Lazzaretto, A. (2011). Numerical simulation of a hydrogen fuelled gas turbine combustor. *International Journal of Hydrogen Energy, 36*(13), 7993–8002.

Han, W., Jin, H., Zhang, N., & Zhang, X. (2007). Cascade utilization of chemical energy of natural gas in an improved CRGT cycle. *Energy, 32*(4), 306–313.

Ismail, A. K., Abdullah, M. Z., Zubair, M., Ahmad, Z. A., Jamaludin, A. R., Mustafa, K. F., & Nazir, A. M. (2013). Application of porous medium burner with micro cogeneration system. *Energy, 50*, 131-142.

Li, L., Peng, X. F., & Liu, T. (2006). Combustion and cooling performance in an aero-engine annular combustor. *Applied Thermal Engineering, 26*(16), 1771–1779.

Luo, C., Zhang, N., Lior, N., & Lin, H. (2011). Proposal and analysis of a dual-purpose system integrating a chemically recuperated gas turbine cycle with thermal seawater desalination. *Energy, 36*(6), 3791–3803.

Mujeebu, M. A., Abdullah, M. Z., & Zubair, M. (2013). Experiment and CFD simulation to develop clean porous medium surface combustor using LPG. *Journal of Thermal Science and Technology, Isi Bilimi ve Teknigi Dergisi/Journal of Thermal Science & Technology, 33*(1), 55-61.

Wang, H., Luo, K., Lu, S., & Fan, J. (2011). Direct numerical simulation and analysis of a hydrogen/air swirling premixed flame in a micro combustor. *International Journal of Hydrogen Energy, 36*(21), 13838–13849.

Zhang, M., Fu, Z., Lin, Y., & Li, J. (2012). CFD Study of NOX emissions in a model commercial aircraft engine combustor. *Chinese Journal of Aeronautics, 25*(6), 854–863.